Journal of Sound and Vibration (2003) **259**(4), 873–891
doi:10.1006/jsvi.2002.5127, available online at http://www.idealibrary.com on IDEAL®

APPLICATION OF THE SPECTRAL FINITE ELEMENT METHOD TO TURBULENT BOUNDARY LAYER INDUCED VIBRATION OF PLATES

F. Birgersson

MWL, Vehicle Engineering, KTH, SE-100 44 Stockholm, Sweden

N. S. Ferguson

*ISVR, The University of Southampton, Southampton SO*17 1*BJ, England*

AND

S. Finnveden

MWL, Vehicle Engineering, KTH, SE-100 44 *Stockholm, Sweden. E-mail: svantef@fkt.kth.se*

(*Received* 26 *October* 2001, *and in final form* 11 *February* 2002)

The spectral finite element method and equally the dynamic stiffness method use exponential functions as basis functions. Thus it is possible to find exact solutions to the homogeneous equations of motion for simple rod, beam, plate and shell structures. Normally, this restricts the analysis to elements where the excitation is at the element ends. This study removes the restriction for distributed excitation, that in particular has an exponential spatial dependence, by the inclusion of the particular solution in the set of basis functions. These elementary solutions, in turn, build up the solution for an arbitrary homogeneous random excitation. A numerical implementation for the vibration of a plate, excited by a turbulent boundary layer flow, is presented. The results compare favourably with results from conventional modal analysis.

1. INTRODUCTION

The vibrations induced by fluctuating flow may lead to structural fatigue [1] and may also be the source of excessive noise. Specifically these fluctuations arise when, at high speeds, a vehicle is propelled through a fluid or when the fluid is transmitted through a duct or pipe. Sometimes the pulsating fluid motion is inherent in the process, e.g., fan and aircraft propellers. In other cases, vortices are created when the fluid motion is not sufficiently streamlined. In all cases, the fluid inertia forces will become greater than the viscous forces and a turbulent boundary layer (TBL) develops if the velocity is high enough and the structure large.

Industries that wish to improve their product's comfort and reliability by simulation of the dynamic response often use the finite element method (FEM). The FEM provides a mathematically stable environment and also allows for a complex geometry of the modelled structure, both of which are essential for industrial application. However, with high-frequency excitation, many structures of interest require impossibly large computer models, which even the rapid evolution of computing power cannot accommodate for

0022-460X/02/$35.00

within a foreseeable future. This is especially true for distributed random excitation, such as TBL excitation, for which the forced response problem requires orders of magnitude more computational effort than the modal analysis of the structure.

The spectral finite element method (SFEM) is a direct FE method, formulated in the frequency domain, based on a variational formulation for non-conservative motion [2, 3]. The frequency-dependent formulation simplifies the inclusion of frequency-dependent material characteristics and boundary conditions. The elements are formulated and assembled as in the standard FEM while the basis functions are exact solutions to the equations of motion. This reduces the number of degrees of freedom and increases the accuracy. The SFEM has been used for studies of vibrations in fluid-filled pipes [4], beam frame works and in beam-stiffened panels in railway cars [5]. An experimental validation of the SFEM for pipes has been presented in reference [6]. The SFEM has many siblings of which the most well known are the direct dynamic stiffness method [7, 8], the exact members method [9, 10] and the spectral element method [11]. The SFEM is special in that it is based on a variational formulation, similar to the standard FEM. The variational formulation seems advantageous when approximate shape functions are used and restraints on motion need be imposed. Otherwise, all the spectral methods seem equivalent and the choice between any of them is a matter of preference.

Normally, the spectral FEM, and equally the dynamic stiffness method, considers excitation at the element ends only. Hence, these methods do not seem suitable for modelling distributed excitation, such as TBL excitation. A remedy for excitation in the form of a plane pressure wave was however proposed by Langley [7], where, besides the homogenous solutions to the equation of motion, the particular solution was included in the set of trial functions. Upon this basis, the nodal equations of motion were formulated and the forced motion described as a function of excitation amplitude and wavenumber. Birgersson examined this approach using the dynamic stiffness method and the spectral FEM [12]. For distributed excitation with a complex exponential spatial dependence, i.e., a plane wave, the responses were calculated for rods, Euler beams, Timoshenko beams, pre-stressed Timoshenko beams on Winkler foundations and simply supported plates. At all stages, the numerical accuracy and stability was confirmed.

The only previous applications for distributed excitations with spectral methods are those by Langley [7] and more recently by Leung [8]. Leung describes the distributed excitation with interpolating FE polynomials instead of a superposition of plane wave excitations. This description may or may not be more efficient than the plane wave description, depending on the form of excitation. For TBL excitation at high frequencies the here-proposed method seems more promising.

Turbulence is an intrinsically non-linear process, which can only be described in statistical terms. The cross-spectral density of the wall pressure is usually the quantity of interest for stationary vibration response prediction and is generally described by semi-empirical models. The most common is attributed to Corcos [13], and has been validated experimentally. It overestimates the wall-pressure cross-spectral density at wavenumbers below the convective peak [14, 15]. Therefore, a number of different models have evolved [16], all of which are of a form that allows prediction with the method investigated here.

The cross-spectral density of the response to random excitation is most often given in terms of a double integral over the surface of the system of the frequency response functions and the cross-spectral density of the pressure [17]. For standard FE calculations, the corresponding summation twice over the surface is very costly. In an alternative approach, given that the excitation is homogenous, the response cross-spectral density is equally determined by a single integration over all wavenumbers. In this case, the integrand is given by the excitation wavenumber–frequency spectrum and the "sensitivity

function'', which is the response of the structure to a pressure wave of unit magnitude [17]. It differs from the joint acceptance function in that it does not consider individual modal responses. The knowledge of this sensitivity function makes it possible to calculate the response of the structure to TBL excitation. This approach is efficient and more informative than the standard approach, since the spatial characteristic of the excitation is directly compared to that of the response.

In what follows, a new method of calculating the response of plates, excited by TBL flow, is presented. First the response of a plate with simply supported and free edges to a distributed pressure with a complex exponential dependence is described. A transverse deflection shape is assumed in order to reduce the governing wave equation to the one-dimensional case. The model developed has been validated in several ways, as outlined in section 3. The TBL is described by a Corcos model and the response of a plate structure to this random excitation is predicted. Finally, the results are favourable compared with results predicted with conventional modal analysis in section 5.

2. SPECTRAL FINITE ELEMENT FORMULATION FOR DISTRIBUTED SOURCES

2.1. EQUATIONS OF MOTION

Consider a thin isotropic plate of length a, width b and thickness h (Figure 1) excited by a plane pressure wave with description $p(x,y,t) = p_0 e^{-i\alpha_x x} e^{-i\alpha_y y} e^{i\omega t}$. The differential equation governing the plate vibrations can be written as, cf., reference [7],

$$D\left(\frac{\partial^4}{\partial x^4} + 2\frac{\partial^2}{\partial x^2}\frac{\partial^2}{\partial y^2} + \frac{\partial^4}{\partial y^4}\right)w - \varrho h\omega^2 w = p_0 e^{-i\alpha_x x} e^{-i\alpha_y y}, \tag{1}$$

where w is the out-of-plane deflection and ϱ is the mass per unit volume. $D = Eh^3/(12(1-\nu^2))$ is the flexural rigidity with E denoting Young's modulus and ν the Poisson ratio. Damping losses are accounted for by the inclusion of a complex Young's modulus $E(1+i\eta)$. Given simply supported boundary conditions along $y = 0$ and b, the deflections can be expanded in the form

$$w(x,y) = \sum_{n=1}^{\infty} X_n(x)\sin(k_n y) \quad \text{with} \quad k_n = \frac{n\pi}{b}. \tag{2}$$

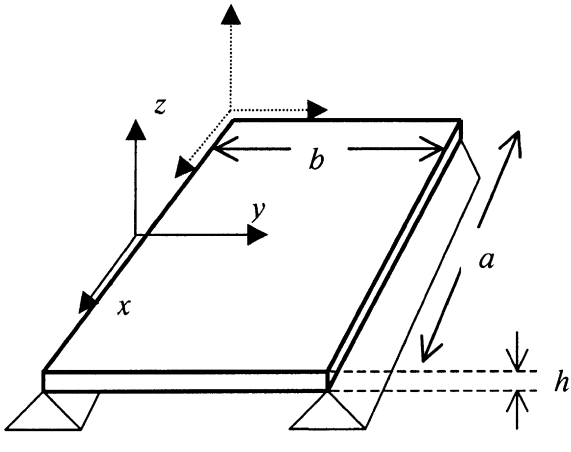

Figure 1. Thin isotropic plate with free and simply supported edges. Dotted line indicates the coordinate system used for modal analysis later.

This solution satisfies the boundary conditions on the two parallel edges $y = 0$ and b. Insert equation (2) into equation (1), multiply with $\sin(k_m y)$ and then integrate with respect to y over the width. Due to orthogonality the left-hand side integral is zero, except if $m = n$. It follows that the deflection is given by

$$D\left(\frac{\mathrm{d}^4 X_n}{\mathrm{d}x^4} - 2k_n^2 \frac{\mathrm{d}^2 X_n}{\mathrm{d}x^2} + k_n^4 X_n\right) - \varrho h\omega^2 X_n = p_x, \tag{3}$$

where

$$p_x = p_0 P_n(\alpha_y) \mathrm{e}^{-\mathrm{i}\alpha_x x}, \tag{4}$$

$$P_n(\alpha_y) = \frac{2}{b}\int_0^b \mathrm{e}^{-\mathrm{i}\alpha_y y} \sin(k_n y)\,\mathrm{d}y. \tag{5}$$

The solution $X_n(x)$ to equation (3) represents a complex amplitude and can be written as a sum of a complementary function and a particular integral in the form

$$X_n(x) = \sum_{i=1}^{4} a_{ni}\mathrm{e}^{k_{ni}x} + X_{np}(x) = \mathrm{e}^{\mathbf{K}x}\mathbf{C}_n + X_{np}(x), \tag{6}$$

$$X_{np}(x) = c_n \mathrm{e}^{-\mathrm{i}\alpha_x x}, \tag{7}$$

where

$$c_n = \frac{p_0 P_n(\alpha_y)}{(D\alpha_x^4 + 2k_n^2 D\alpha_x^2 + Dk_n^4 - \varrho h\omega^2)}, \tag{8}$$

$$\mathbf{K} = (\, k_{n1} \quad k_{n3} \quad k_{n2} \quad k_{n4}\,), \quad \mathbf{C}_n = (\, C_{n1} \quad C_{n2} \quad C_{n3} \quad C_{n4}\,)^{\mathrm{T}}. \tag{9}$$

The convention that the exponential of a vector produces a vector with the exponential of each term is adopted here. k_{ni} are the four roots to the following dispersion relationship for k,

$$Dk_{ni}^4 - 2Dk_n^2 k_{ni}^2 + Dk_n^4 - \varrho h\omega^2 = 0, \tag{10}$$

with the roots $k_{n1,n2} = \pm\sqrt{k_n^2 + k^2}$ and $k_{n3,n4} = \pm\sqrt{k_n^2 - k^2}$, $k^2 = \sqrt{\varrho h\omega^2/D}$. To ensure numerical stability, when $\mathrm{e}^{k_{ni}l_x}$ or $\mathrm{e}^{-k_{ni}l_x}$ is large, solution (6) is scaled, see reference [5]:

$$X_n(x) = \mathrm{e}^{\mathbf{K}x - \mathbf{K}_p l_x}\mathbf{C}_n + c_n \mathrm{e}^{-\mathrm{i}\alpha_x x}, \tag{11}$$

where

$$l_x = a/2, \tag{12}$$

$$(\mathbf{K}_p)_i = \begin{cases} -\mathbf{K}_i, & \mathrm{Re}(\mathbf{K}_i) \leqslant 0, \\ \mathbf{K}_i, & \text{else.} \end{cases} \tag{13}$$

The unknown constants C_{ni} are related to the boundary conditions at the ends of the plate by

$$\begin{pmatrix} X_n(-l_x) \\ X_n'(-l_x) \\ X_n(+l_x) \\ X_n'(+l_x) \end{pmatrix} = \begin{pmatrix} \mathrm{e}^{\mathbf{K}(-l_x) - \mathbf{K}_p l_x} \\ \mathbf{K}. * \mathrm{e}^{\mathbf{K}(-l_x) - \mathbf{K}_p l_x} \\ \mathrm{e}^{\mathbf{K}(+l_x) - \mathbf{K}_p l_x} \\ \mathbf{K}. * \mathrm{e}^{\mathbf{K}(+l_x) - \mathbf{K}_p l_x} \end{pmatrix} \begin{pmatrix} C_{n1} \\ C_{n2} \\ C_{n3} \\ C_{n4} \end{pmatrix} + \begin{pmatrix} X_{np}(-l_x) \\ -\mathrm{i}\alpha_x X_{np}(-l_x) \\ X_{np}(+l_x) \\ -\mathrm{i}\alpha_x X_{np}(+l_x) \end{pmatrix}, \tag{14}$$

where $.*$ denotes element-wise multiplication (as in MATLAB) and a prime denotes differentiation with respect to x. Equation (14) can be solved for $\mathbf{C}_n$,

$$\mathbf{C}_n = \mathbf{A}(\mathbf{W}_n - \mathbf{W}_{nc}), \tag{15}$$

where

$$\mathbf{A} = \begin{pmatrix} \mathrm{e}^{\mathbf{K}(-l_x)-\mathbf{K}_p l_x} \\ \mathbf{K}.*\mathrm{e}^{\mathbf{K}(-l_x)-\mathbf{K}_p l_x} \\ \mathrm{e}^{\mathbf{K}(+l_x)-\mathbf{K}_p l_x} \\ \mathbf{K}.*\mathrm{e}^{\mathbf{K}(+l_x)-\mathbf{K}_p l_x} \end{pmatrix}^{-1}, \quad \mathbf{W}_n = \begin{pmatrix} X_n(-l_x) \\ X_n'(-l_x) \\ X_n(+l_x) \\ X_n'(+l_x) \end{pmatrix}, \quad \mathbf{W}_{nc} = \begin{pmatrix} X_{np}(-l_x) \\ -\mathrm{i}\alpha_x X_{np}(-l_x) \\ X_{np}(+l_x) \\ -\mathrm{i}\alpha_x X_{np}(+l_x) \end{pmatrix}. \tag{16}$$

Insert equation (15) into equation (11) to obtain the complex amplitude $X_n(x)$,

$$X_n(x) = \mathrm{e}^{\mathbf{K}x-\mathbf{K}_p l_x}\mathbf{A}(\mathbf{W}_n - \mathbf{W}_{nc}) + c_n \mathrm{e}^{-\mathrm{i}\alpha_x x} = \mathrm{e}^{\mathbf{K}x-\mathbf{K}_p l_x}\mathbf{A}\mathbf{W}_n + c_n \mathrm{e}^{\boldsymbol{\alpha}_\mathbf{K} x-\boldsymbol{\alpha}_{\mathbf{K}p} l_x}\mathbf{W}_{np}, \tag{17}$$

where

$$\mathbf{K} = (\, k_{n1} \quad k_{n3} \quad k_{n2} \quad k_{n4} \,),$$

$$\boldsymbol{\alpha}_\mathbf{K} = (\, \mathbf{K} \quad -\mathrm{i}\alpha_x \,), \quad \boldsymbol{\alpha}_{\mathbf{K}p} = (\, \mathbf{K}_p \quad 0 \,),$$

$$\mathbf{W}_{np} = (\, W_{np1} \quad W_{np2} \quad \ldots \quad W_{np5} \,)^{\mathrm{T}}, \quad (W_{np})_{1,\ldots,4} = -\mathbf{A}\mathbf{W}_{nc}/c_n, \quad (W_{np})_5 = 1. \tag{18}$$

Equations (17) and (2) together give the exact shape functions to the governing differential equation (1) for all plane travelling pressure waves of the form $p_0 \mathrm{e}^{-\mathrm{i}\alpha_x x}\mathrm{e}^{-\mathrm{i}\alpha_y y}\mathrm{e}^{\mathrm{i}\omega t}$.

2.2. VARIATIONAL PRINCIPLE FOR DISTRIBUTED PRESSURE

2.2.1. *Plate formulation*

For free wave motion and with damping neglected, Hamilton's principle in the time domain applies

$$\int_{t_1}^{t_2} \delta(U - T)\,\mathrm{d}t = \int_{t_1}^{t_2} \delta(L)\,\mathrm{d}t = 0, \tag{19}$$

where T and U are the kinetic and elastic strain energies. The functional $(U - T)$ will here be referred to as virtual work and later as the Lagrangian L. To study wave propagation in the frequency domain, assuming a harmonic and stationary time dependence, one lets $t_{1,2} \to \pm\infty$ and apply Parseval's identity. The governing equations are linear and thus the different frequency components in the resulting integral do not couple with each other. The integrand is zero for all frequencies and the virtual work is stationary for each frequency. For free harmonic vibrations of the form $\mathrm{e}^{\mathrm{i}\omega t}$, the virtual work of the element for the out-of-plane displacement is given by the following bi-linear functional [18, p. 35]:

$$L = \int_{-l_x}^{l_x} \mathrm{d}x \int_0^b \left\{ \frac{h^3}{12}(\boldsymbol{\varepsilon}^*)^{\mathrm{T}}\mathbf{D}\boldsymbol{\varepsilon} - \varrho h\omega^2 w^* w \right\} \mathrm{d}y, \tag{20}$$

where $\boldsymbol{\varepsilon}$ and the stiffness matrix $\mathbf{D}$ are defined as

$$\boldsymbol{\varepsilon} = \left(\frac{\partial^2 w}{\partial x^2} \quad \frac{\partial^2 w}{\partial y^2} \quad 2\frac{\partial^2 w}{\partial x \partial y} \right)^{\mathrm{T}}, \quad \mathbf{D} = \frac{12}{h^3}\begin{pmatrix} D & Dv & 0 \\ Dv & D & 0 \\ 0 & 0 & D(1-v)/2 \end{pmatrix}. \tag{21}$$

The asterisk denotes the complex conjugate and $w(x, y, \omega)$ is the transverse displacement. With dissipative losses, equation (20) no longer has a stationary minimum for the displacement functions. As discussed by Finnveden [5], these losses may be attributed by employing a variational principle similar to that of Hamilton. Thus, the bi-linear forms in the displacement w and its complex conjugate w^* are replaced with bi-linear forms in the displacement w and in the complex conjugates of the displacement w^a in an

adjoint negatively damped system [2, 3]. This is conceptually more complex but the approach requires no extra calculation effort. The virtual work of the distributed pressure $p(x, y)$ is also included, as in reference [12] for example, producing the Lagrangian

$$L = \int_{-l_x}^{l_x} \mathrm{d}x \int_0^b \left\{ \frac{h^3}{12} (\boldsymbol{\varepsilon}^a)^T \mathbf{D} \boldsymbol{\varepsilon} - \varrho h \omega^2 w^a w - p^* w - p w^a \right\} \mathrm{d}y. \tag{22}$$

2.2.2. *Trial functions for plate with two opposite edges simply supported*

The displacement functions and also the trial functions, given simply supported boundary conditions, are expressed by equation (2) as a modal sum. The displacement functions for the adjoint system are similarly given as a modal sum.

$$w(x, y) = \sum_{n=1}^{\infty} X_n(x) \sin(k_n y), \quad \text{where } X_n(x) = \mathrm{e}^{\mathbf{K} x - \mathbf{K}_p l_x} \mathbf{A} \mathbf{W}_n + c_n \mathrm{e}^{\boldsymbol{\alpha}_\mathbf{K} x - \boldsymbol{\alpha}_{\mathbf{K}_p} l_x} \mathbf{W}_{np}, \tag{23}$$

$$w^a(x, y) = \sum_{n=1}^{\infty} X_n^a(x) \sin(k_n y), \quad \text{where } X_n^a(x) = \mathrm{e}^{\mathbf{K} x - \mathbf{K}_p l_x} \mathbf{A} \mathbf{W}_n^a + c_n \mathrm{e}^{\boldsymbol{\alpha}_\mathbf{K} x - \boldsymbol{\alpha}_{\mathbf{K}_p} l_x} \mathbf{W}_{np}. \tag{24}$$

Equation (24) defines the test functions that are to be varied to find the displacement functions, described by equation (23). These functions are substituted into equation (22) and the integral over y is evaluated. Due to orthogonality, the Lagrangian L is reduced to a number of one-dimensional L_n. For each of these, the first variation with respect to the test functions has to be zero. The pressure, described by $p(x, y, t) = p_0 \mathrm{e}^{-\mathrm{i}\alpha_x x} \mathrm{e}^{-\mathrm{i}\alpha_y y} \mathrm{e}^{\mathrm{i}\omega t}$, is substituted into the Lagrangian. The procedure outlined is similar to a Galerkin procedure, cf. reference [19],

$$\begin{aligned} L_n = \frac{b}{2} \int_{-l_x}^{l_x} \Big\{ & (\mathrm{d}^2 X_n^a / \mathrm{d}x^2)^{\mathrm{T}} B_1 (\mathrm{d}^2 X_n / \mathrm{d}x^2) + (\mathrm{d}^2 X_n^a / \mathrm{d}x^2)^{\mathrm{T}} B_2 (X_n) \\ & + (X_n^a)^{\mathrm{T}} B_2 (\mathrm{d}^2 X_n / \mathrm{d}x^2) + (\mathrm{d}X_n^a / \mathrm{d}x)^{\mathrm{T}} B_3 (\mathrm{d}X_n / \mathrm{d}x) \\ & + (X_n^a)^{\mathrm{T}} B_4 (X_n) - (X_n^a)^{\mathrm{T}} p_x - p_x^*(X_n) \Big\} \mathrm{d}x, \end{aligned} \tag{25}$$

where $B_1 = D$, $B_2 = -D\nu k_n^2$, $B_3 = 2D(1 - \nu) k_n^2$ and $B_4 = D k_n^4 - \varrho h \omega^2$.

2.2.3. *Derivation of nodal displacement*

Equation (25) is evaluated by substituting the functions X_n and X_n^a, and their respective derivatives, into it. By requiring that the first variation of the Lagrangian with respect to the variational parameters $\mathbf{W}_n^a$ is zero, a system of equations for the nodal displacement $\mathbf{W}_n$ is found.

$$\mathbb{D}_n \mathbf{W}_n = \mathbf{F}_n, \tag{26}$$

where the dynamic stiffness matrix $\mathbb{D}_n$ and the forcing $\mathbf{F}_n$ are detailed in Appendix A together with a derivation of the quantities. The element formulation given by equation (26) is exact, which means that there is no need for numerical quadrature. The formulation applies equally for other boundary conditions at the free edges, such as clamped, simply supported, etc. The dynamic stiffness matrix $\mathbb{D}_n$ does not depend on the excitation and for a general source, described by a superposition of plane wave pressure excitations, it is therefore only the nodal force vector $\mathbf{F}_n$ that needs to be recalculated.

Solving equation (26) gives the nodal displacements $\mathbf{W}_n$ of the structure, when excited by a plane pressure wave of the form $p_0 \mathrm{e}^{-\mathrm{i}\boldsymbol{\alpha}\mathbf{s}} = p_0 \mathrm{e}^{-\mathrm{i}\alpha_x x} \mathrm{e}^{-\mathrm{i}\alpha_y y}$. Given $\mathbf{W}_n$, equations (17) and (2) together give the total response of the structure at any position $\mathbf{r}$.

For future reference the response to a pressure wave with $p_0 = 1\,\mathrm{N/m^2}$ will here be denoted by the sensitivity function $G(\mathbf{r}, \boldsymbol{\alpha}, \omega)$. This function may also be expressed as an integral

$$G(\mathbf{r}, \boldsymbol{\alpha}, \omega) = \int_R H(\mathbf{r}, \mathbf{s}, \omega) \mathrm{e}^{-\mathrm{i}\boldsymbol{\alpha}\mathbf{s}} \, \mathrm{d}\mathbf{s}, \tag{27}$$

where $H(\mathbf{r}, \mathbf{s}, \omega)$ is the displacement at location $\mathbf{r}$ resulting from a point force of unit magnitude applied at location $\mathbf{s}$.

3. VALIDATION OF THE DEVELOPED MODELS

3.1. COMPARISON WITH THE DYNAMIC STIFFNESS METHOD (DSM)

With the DSM it is possible to describe the response to distributed pressure with exponential dependence, see reference [7] for a plate and reference [12] for a rod, various beams, including for example pre-stressed and elastic foundation, and plates. For all these cases the DSM and SFEM produce the same system of equations for distributed pressure. The way the methods calculate the dynamic stiffness matrices differ and because of this, there are some numerical differences for large and small Helmholtz numbers kl_x, as discussed in reference [12].

3.2. RESPONSE TO A POINT FORCE

To validate the expressions derived so far and to develop an understanding for the convergence of results for arbitrary excitation, the response of a simply supported plate to a point force was investigated. The simply supported plate is detailed in section 5.1. The point force f is approximated with a finite spatial Fourier series and the response to each term in this series is calculated with the models developed. Superposition is valid as wave equation (1) is linear and the final response is a sum of all responses. This response is compared to the exact response calculated with a dynamic stiffness method, outlined in Appendix B.

Similar to the equations of motion of the plate, the force is decomposed into a series of half sine waves in the y direction. In the x direction the force is described by an exponential Fourier series:

$$f(x,y) = F_0 \delta(x - x_s)\delta(y - y_s) \approx \frac{F_0}{2l_x} \sum_{m'=-M'}^{M'} \mathrm{e}^{\mathrm{i}2m'\pi x/2l_x} \mathrm{e}^{-\mathrm{i}2m'\pi x_s/2l_x} \frac{2}{b} \sum_{n'=1}^{N'} \sin\left(\frac{n'\pi y}{b}\right) \sin\left(\frac{n'\pi y_s}{b}\right), \tag{28}$$

for large values of M' and N'. The convergence of the series is illustrated in Figure 2, where a point force of unit magnitude, applied at $x_s = 0$ and $y_s = b/3$, is approximated with $N' = 10$ and either $M' = 1$ (left) or $M' = 5$ (right).

Equation (28) is substituted as the pressure $p(x, y)$ into equation (1). For a given m' and transverse mode n, $p_x = F_0(\sin(n\pi y_s/b)\mathrm{e}^{-\mathrm{i}2m'\pi x_s/2l_x}/l_x b)\mathrm{e}^{-\mathrm{i}(2m'\pi/2l_x)x}$. Figure 3 shows the resulting plate mean square velocity with the described pressure excitation and also the exact response to the point force calculated from equation (B2). The relative error in velocity decreases as more terms are considered, see Figure 4. With $M' = 100$, i.e., considering 201 terms, the relative error is less than 0·1%. The relative error depends on the wavenumber kl_x and increases with frequency as increasing higher order modes are necessary to describe the response.

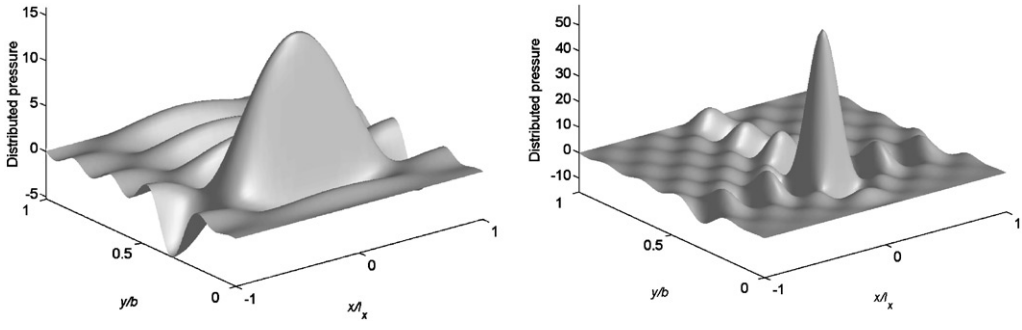

Figure 2. Point force of unit magnitude approximated as a distributed pressure. Left, $M' = 1$, $N' = 10$. Right, $M' = 5$, $N' = 10$.

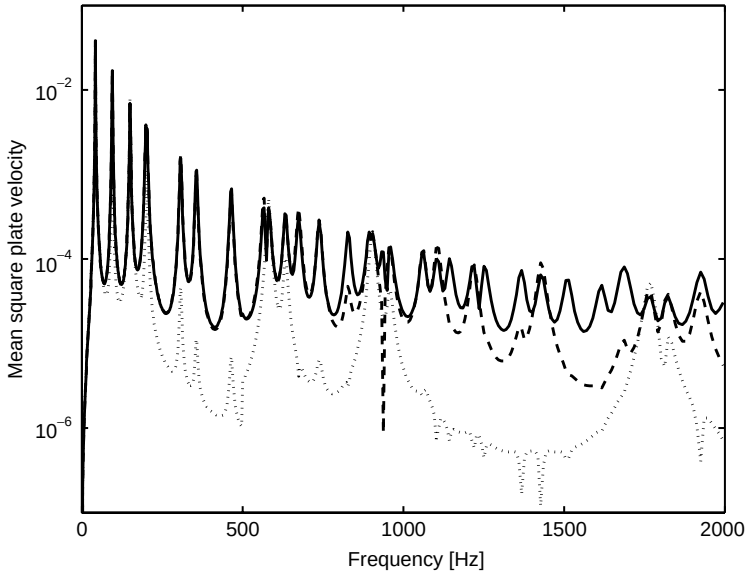

Figure 3. Mean square plate velocity: (—) point force and equally distributed excitation with $M' = 100$; (– –) distributed excitation with $M' = 5$; (· · · · · ·) distributed excitation with $M' = 1$.

4. PLATE RESPONSE TO TBL EXCITATION

In this section the cross-spectral density of the response is expressed as an integral of the sensitivity function and the cross-spectral density of the turbulent boundary layer (TBL) wall pressure. The sensitivity function of the plate structure was calculated in section 2.

The integral usually has to be calculated numerically, which decreases efficiency. By expressing the cross-spectral density of the TBL wall pressure as a Fourier series, instead of using the Fourier transform, a new approach is derived. The integral is replaced by a summation.

4.1. CROSS-SPECTRAL DENSITY OF THE PRESSURE

The TBL wall pressure is described by the Corcos model [13]. From a curve fit for the narrow-band spatial correlation between wall pressures, Corcos obtained the

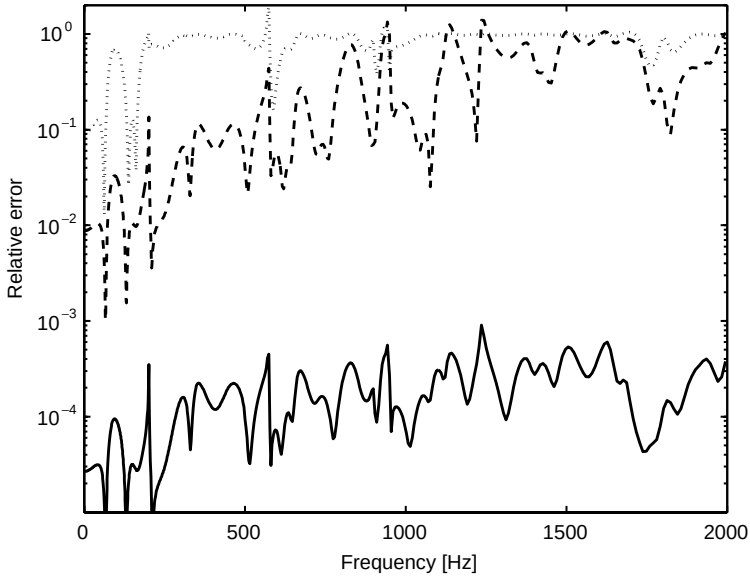

Figure 4. Relative error of mean square plate velocity: (—) distributed excitation with $M' = 100$; (– –) distributed excitation with $M' = 5$; (· · · · · ·) distributed excitation with $M' = 1$.

cross-spectral density of the pressure

$$\langle p^*(x_s, y_s, \omega) p(x'_s, y'_s, \omega) \rangle \tag{29}$$

$$= S_{pp}(\xi_x, \xi_y, \omega) = \Phi_{pp}(\omega) \exp\left(-c_x \left|\frac{\omega \xi_x}{U_c}\right|\right) \exp\left(-c_y \left|\frac{\omega \xi_y}{U_c}\right|\right) \exp\left(\frac{\mathrm{i}\omega \xi_x}{U_c}\right), \tag{30}$$

where

$$\xi_x = x_s - x'_s \quad \text{and} \quad \xi_y = y_s - y'_s. \tag{31}$$

$\langle\ \rangle$ denotes statistical expectation, c_x and c_y are constants describing the spatial coherence of the wall pressure field, in the longitudinal and transverse directions, respectively, and U_c is the convection velocity.

4.2. FOURIER TRANSFORM

It is assumed that the distributed random excitation is stationary in time. Considering the case when there are N separate input forces at position $\mathbf{s}_i$, the cross-spectral density between the response at position $\mathbf{r}_1$ and the response at position $\mathbf{r}_2$ is given by Newland [7, Chapter 16] as

$$S_{ww}(\mathbf{r}_1, \mathbf{r}_2, \omega) = \sum_{j=1}^{N} \sum_{k=1}^{N} H^*(\mathbf{r}_1, \mathbf{s}_j, \omega) H(\mathbf{r}_2, \mathbf{s}_k, \omega) S_{ff}(\mathbf{s}_j, \mathbf{s}_k, \omega), \tag{32}$$

where

$$\mathbf{r} = (\,x \quad y\,)^{\mathrm{T}}, \quad \mathbf{s}_1 = (\,x_s \quad y_s\,)^{\mathrm{T}}, \quad \mathbf{s}_2 = (\,x'_s \quad y'_s\,)^{\mathrm{T}}. \tag{33}$$

$S_{ff}(\mathbf{s}_j, \mathbf{s}_k, \omega)$ is the force cross-spectral density and $H(\mathbf{r}, \mathbf{s}, \omega)$ is the displacement at location $\mathbf{r}$ resulting from a point force of unit magnitude applied at location $\mathbf{s}$. When the number of

input forces becomes infinite, as is the case for a fluctuating pressure field, then the summations become integrals over the surface,

$$S_{ww}(\mathbf{r}_1, \mathbf{r}_2, \omega) = \int_R \int_R H^*(\mathbf{r}_1, \mathbf{s}_1, \omega) H(\mathbf{r}_2, \mathbf{s}_2, \omega) S_{pp}(\mathbf{s}_1, \mathbf{s}_2, \omega) \mathrm{d}\mathbf{s}_1 \, \mathrm{d}\mathbf{s}_2. \tag{34}$$

This equation gives the cross-spectral density between the responses $w(\mathbf{r}_1, \omega)$ and $w(\mathbf{r}_2, \omega)$ in terms of a double integral over the surface of the system of the frequency response functions and the cross-spectral density of the pressure $S_{pp}(\mathbf{s}_1, \mathbf{s}_2, \omega)$.

Now, consider the case when the distributed excitation $p(\mathbf{s}, t)$ is a sample function from a process that is homogeneous in space. Then the cross-spectral density $S_{pp}(\mathbf{s}_j, \mathbf{s}_k, \omega)$ is related to the wavenumber cross-spectral density $S_{PP}(\boldsymbol{\alpha}, \omega)$ by

$$S_{pp}(\mathbf{s}_j, \mathbf{s}_k, \omega) = \int_\infty S_{PP}(\boldsymbol{\alpha}, \omega) \mathrm{e}^{\mathrm{i}(\boldsymbol{\alpha}(\mathbf{s}_k - \mathbf{s}_j))} \, \mathrm{d}\boldsymbol{\alpha}, \tag{35}$$

where $\boldsymbol{\alpha}$ is a wave vector. Substituting expression (35) into equation (34) and changing the order of integration gives

$$S_{ww}(\mathbf{r}_1, \mathbf{r}_2, \omega) = \int_\infty G^*(\mathbf{r}_1, -\boldsymbol{\alpha}, \omega) G(\mathbf{r}_2, -\boldsymbol{\alpha}, \omega) S_{PP}(\boldsymbol{\alpha}, \omega) \, \mathrm{d}\boldsymbol{\alpha}, \tag{36}$$

where the sensitivity function $G(\mathbf{r}, \boldsymbol{\alpha}, \omega)$ is defined by equation (27) as the response to a plane pressure wave of the form $p_0 \mathrm{e}^{-\mathrm{i}\boldsymbol{\alpha}\mathbf{s}}$, with $p_0 = 1 \, \mathrm{N/m^2}$.

4.3. FOURIER SERIES

Equation (34) will be evaluated. The cross-spectral density of the pressure $S_{pp}(\xi_x, \xi_y, \omega)$ described by equation (30) is expressed as an exponential Fourier series. The period is twice the length of the plate as the integral of ξ_x and ξ_y needs to be evaluated in the interval $-2l_x, \ldots, 2l_x (= -a, \ldots, a)$ and $-b, \ldots, b$. Outside this interval, the cross-spectral density can be made periodic because any existing pressure outside the integration limits will not influence the result. Upon this basis, the cross-spectral density is given by

$$S_{pp}(\xi_x, \xi_y, \omega) = \Phi_{pp}(\omega) \sum_{m'} S_{PPx}(\alpha_{m'}) \mathrm{e}^{\mathrm{i}\alpha_{m'}\xi_x} \sum_{n'} S_{PPy}(\alpha_{n'}) \mathrm{e}^{\mathrm{i}\alpha_{n'}\xi_y}, \tag{37}$$

where

$$\alpha_{m'} = 2\pi m'/2a, \quad \alpha_{n'} = 2\pi n'/2b. \tag{38}$$

For the Corcos model in equation (37), the Fourier coefficients $S_{PPx}(\alpha_{m'})$ and $S_{PPy}(\alpha_{n'})$ are given by

$$S_{PPx}(\alpha_{m'}) = \frac{1}{2a} \int_{-a}^{a} \mathrm{e}^{-c_x \omega |\xi_x| / U_c} \mathrm{e}^{\mathrm{i}\omega(\xi_x)/U_c} \mathrm{e}^{-\mathrm{i}\alpha_{m'}\xi_x} \, \mathrm{d}\xi_x = \frac{1}{2a} \left(\frac{1 - \mathrm{e}^{-d_1 a}}{d_1} + \frac{\mathrm{e}^{d_2 a} - 1}{d_2} \right),$$

$$d_1 = c_x \omega / U_c + \mathrm{i}\omega / U_c - \mathrm{i}\alpha_{m'}, \quad d_2 = -c_x \omega / U_c + \mathrm{i}\omega / U_c - \mathrm{i}\alpha_{m'}, \tag{39}$$

$$S_{PPy}(\alpha_{n'}) = \frac{1}{2b} \int_{-b}^{b} \mathrm{e}^{-c_y \omega |\xi_y| / U_c} \mathrm{e}^{-\mathrm{i}\alpha_{n'}\xi_y} \, \mathrm{d}\xi_y = \frac{1}{2b} \left(\frac{1 - \mathrm{e}^{-d_3 b}}{d_3} + \frac{\mathrm{e}^{d_4 b} - 1}{d_4} \right), \tag{40}$$

$$d_3 = c_y \omega / U_c - \mathrm{i}\alpha_{n'}, \quad d_4 = -c_y \omega / U_c - \mathrm{i}\alpha_{n'}.$$

The series in equation (37) is inserted into equation (34) and the order of summation and integration interchanged:

$$\begin{aligned} S_{ww}(\mathbf{r}_1,\mathbf{r}_2,\omega) &= \int_R\int_R H^*(\mathbf{r}_1,\mathbf{s}_1,\omega)H(\mathbf{r}_2,\mathbf{s}_2,\omega)\Phi_{pp}(\omega)\sum_{m'} S_{PPx}(\alpha_{m'})\mathrm{e}^{\mathrm{i}\alpha_{m'}\xi_x} \\ &\quad\times\sum_{n'} S_{PPy}(\alpha_{n'})\mathrm{e}^{\mathrm{i}\alpha_{n'}\xi_y}\,\mathrm{d}\mathbf{s}_1\,\mathrm{d}\mathbf{s}_2 \\ &= \Phi_{pp}(\omega)\sum_{m'}\sum_{n'} S_{PP}(\boldsymbol{\alpha}_{m'n'})\int_R\int_R (H(\mathbf{r}_1,\mathbf{s}_1,\omega)\mathrm{e}^{-\mathrm{i}\alpha_{m'}x_s}\mathrm{e}^{-\mathrm{i}\alpha_{n'}y_s})^* \\ &\quad\times (H(\mathbf{r}_2,\mathbf{s}_2,\omega)\mathrm{e}^{-\mathrm{i}\alpha_{m'}x_s'}\mathrm{e}^{-\mathrm{i}\alpha_{n'}y_s'})\,\mathrm{d}\mathbf{s}_1\,\mathrm{d}\mathbf{s}_2 \\ &= \Phi_{pp}(\omega)\sum_{m'}\sum_{n'} S_{PP}(\boldsymbol{\alpha}_{m'n'})G^*(\mathbf{r}_1,\boldsymbol{\alpha}_{m'n'},\omega)G(\mathbf{r}_2,\boldsymbol{\alpha}_{m'n'},\omega), \end{aligned} \tag{41}$$

where $\boldsymbol{\alpha}_{m'n'} = (\alpha_{m'}\ \alpha_{n'})$ and $S_{PP}(\boldsymbol{\alpha}_{m'n'}) = S_{PPx}(\alpha_{m'})S_{PPy}(\alpha_{n'})$. The sensitivity function $G(\mathbf{r},\boldsymbol{\alpha},\omega)$ is defined by equation (27). Only a finite number of terms will be considered later, e.g., $m = -M',\ldots,M'$. Given the simply supported plate, $G(\mathbf{r},\boldsymbol{\alpha},\omega)$ is described in section 2 as a sum of the transverse sinusoidal modes $\sin(k_n y)$ and therefore a complete expression for the auto-spectral density of the response is

$$S_{ww}(\mathbf{r},\omega) = \Phi_{pp}(\omega)\sum_{m'=-M'}^{M'}\sum_{n'=-N'}^{N'} S_{PP}(\boldsymbol{\alpha}_{m'n'})\left|\sum_{n=1}^{N} G_n(x,\boldsymbol{\alpha}_{m'n'},\omega)\sin(k_n y)\right|^2. \tag{42}$$

4.4. MODAL APPROACH

For comparison, the total response of a simply supported plate to a harmonic point force $F_0\mathrm{e}^{\mathrm{i}\omega t}$ at $\mathbf{s}_1$ can be expressed as a modal summation

$$w(\mathbf{r}) = \sum_{m=-M}^{M}\sum_{n=-N}^{N}\frac{F_0\ \Psi_{mn}(\mathbf{s}_1)}{\varrho h(\omega_{mn}^2(1+\mathrm{i}\eta)-\omega^2)}\Psi_{mn}(\mathbf{r}), \tag{43}$$

where

$$\Psi_{mn}(x_s,y_s) = \frac{2}{\sqrt{ab}}\sin(k_m x_s)\sin(k_n y_s),$$

$$k_m = \frac{m\pi}{a},\quad k_n = \frac{n\pi}{b}\quad\text{and}\quad \omega_{mn} = \sqrt{\frac{D_0}{\rho h}}(k_m^2+k_n^2). \tag{44}$$

The function H in equation (34) is the response to point force excitation with unit magnitude. Substituting the appropriate expression for H, here described by equation (43), into equation (34) gives the auto-spectral density of the displacement as

$$\begin{aligned} S_{ww}(\mathbf{r},\omega) = \sum_{p=-P}^{P}\sum_{q=-Q}^{Q}\sum_{m=-M}^{M}\sum_{n=-N}^{N}\int_R\int_R &\left(\frac{\Psi_{mn}(\mathbf{s}_1)}{\varrho h(\omega_{mn}^2(1+\mathrm{i}\eta)-\omega^2)}\Psi_{mn}(\mathbf{r})\right)^* \\ &\left(\frac{\Psi_{pq}(\mathbf{s}_2)}{\varrho h(\omega_{pq}^2(1+\mathrm{i}\eta)-\omega^2)}\Psi_{pq}(\mathbf{r})\right)S_{pp}(\mathbf{s}_1,\mathbf{s}_2,\omega)\,\mathrm{d}\mathbf{s}_1\,\mathrm{d}\mathbf{s}_2. \end{aligned} \tag{45}$$

Note that equation (45) requires a double summation over modes (assuming the integral can be evaluated analytically), whereas equation (42) only requires a single summation

over the transverse modes and a single summation over terms from the Fourier series expansion of the pressure.

In case the integral in equation (45) is calculated numerically, the order of summation and integration can be interchanged, replacing the double summation over modes with two single summations instead. The computational effort increases rapidly though, as the double integral is replaced by a double summation over excitation points. Hence this case was not further investigated here.

With the assumption that the modes are not coupled by the forcing field, equation (45) may be reduced. This is often done in literature, see for example references [20, 21], but the approximation is not always recommended. A study by Dahlberg [22] demonstrates a relative error for the r.m.s beam deflection of up to 60%, when cross-modal terms were neglected. The frequency ranges investigated also covered many resonance frequencies.

In the case of a simply supported plate, the double integral over the surface of the plate can be evaluated analytically and in order to compare the results as exactly as possible with the spectral FEM, it is necessary to include the cross-modal terms. In section 5 the response given by the modal analysis was taken as the datum solution. The convergence was verified up to four significant digits at 2000 Hz.

5. NUMERICAL INVESTIGATION

5.1. NUMERICAL TEST CASE

The foregoing theory was applied to a simply supported aluminium plate with properties as follows: dimensions $a = 768\,\text{mm}$, $b = 328\,\text{mm}$, $h = 1{\cdot}6\,\text{mm}$, $\eta = 0{\cdot}02$, $E = 7{\cdot}1 \times 10^{10}\,\text{N/m}^2$, $\nu = 0{\cdot}3$, $\varrho = 2750\,\text{kg/m}^3$. The response was calculated at point $\mathbf{r}$ with co-ordinates $x = 0{\cdot}1\,\text{m}$ and $y = 0{\cdot}2\,\text{m}$, if not otherwise stated. The TBL wall pressure is modelled with equation (30), $U_c = 92\,\text{m/s}$, $c_x = 0{\cdot}116$, $c_y = 0{\cdot}7$ and $\Phi_{pp}(f) = 1\,\text{Pa}^2/\text{Hz}$.

5.2. SENSITIVITY FUNCTION AND MATCHING OF WAVENUMBERS

The aim is to predict the auto-spectral density of the displacement S_{ww} of the plate. According to equation (41) it is given as a summation of terms of the form $S_{PP}(\boldsymbol{\alpha}_{m'n'})|G(\mathbf{r}, \boldsymbol{\alpha}_{m'n'}, \omega)|^2$, where S_{PP} describes the excitation and G the response of the structure. These quantities will be investigated separately. At a given frequency, S_{ww} is given by the multiplication in the wavenumber domain of these with each other and a constant $\Phi_{pp}(\omega)$.

Whenever the structural wavenumber k_{mn} of mode Ψ_{mn} matches the wavenumber of the excitation $\boldsymbol{\alpha}_{m'n'}$, the modal response increases (cf., coincidence effect). If the frequency of the excitation is close to a resonance frequency f_{mn} of the structural mode Ψ_{mn} and the excitation is chosen as $\boldsymbol{\alpha}_{m'=m,n'=n}$, the response of the plate is greatly increased. All natural frequencies up to 1000 Hz are listed in Table 1.

In Figure 5 (left) the squared magnitude response of the structure to a distributed pressure $p_0 e^{-i\alpha_{m'}x} e^{-i\alpha_{n'}y}$, with $p_0 = 1\,\text{N/m}^2$, is examined at 201 Hz. Both the modes $\Psi_{m=5,n=1}$ and $\Psi_{m=3,n=2}$ have natural frequencies close to 201 Hz and their structural wavenumbers closely match the wavenumber of the excitation $\boldsymbol{\alpha}_{m'=5,n'=1}$ and $\boldsymbol{\alpha}_{m'=3,n'=2}$ respectively. These wavenumbers are indicated in the figure. Furthermore, all first order transverse modes respond noticeably to wave excitation with $\boldsymbol{\alpha}_{m',n'=0}$, i.e., a plane pressure wave travelling in the x direction, and so also mode $\Psi_{m=5,n=1}$. All even numbered

TABLE 1

All flexural natural frequencies below 1000 *Hz of the simply supported plate, described in section* 5.1

f_{mn} (Hz)	n				
	1	2	3	4	5
$m = 1$	42	150	330	581	905
$m = 2$	62	170	349	601	924
$m = 3$	95	203	382	634	957
$m = 4$	141	249	428	680	
$m = 5$	200	308	487	739	
$m = 6$	272	380	559	811	
$m = 7$	357	464	644	896	
$m = 8$	455	563	743	994	
$m = 9$	567	674	854		
$m = 10$	691	799	979		
$m = 11$	829	937			
$m = 12$	979				

Note: n denotes transverse order in the y direction and m the longitudinal order.

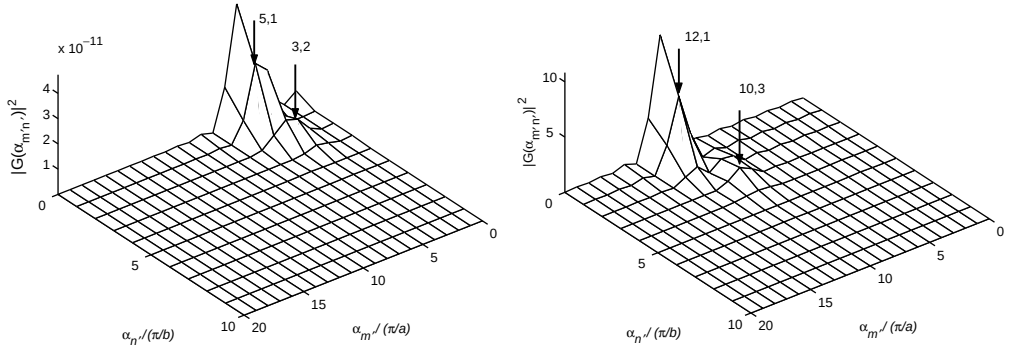

Figure 5. The squared magnitude of the sensitivity function G, describing the response of the structure to distributed pressure $p_0 e^{-i\alpha_{m'}x} e^{-i\alpha_{n'}y}$, where m' and n' are integer values and $p_0 = 1\,\mathrm{N/m^2}$. Left, 201 Hz. Right, 981 Hz.

transverse modes on the other hand, e.g., $\Psi_{m=3,n=2}$, are not excited as $P_{n=2,4,\ldots}(\alpha_y = 0) = 0$, see equation (5).

At higher frequencies other modes dominate the response. Both modes $\Psi_{m=12,n=1}$ and $\Psi_{m=10,n=3}$ have natural frequencies f_{mn} close to 981 Hz and respond strongly at this frequency when excited by $\boldsymbol{\alpha}_{m'=12,n'=1}$ and $\boldsymbol{\alpha}_{m'=10,n'=3}$ respectively, cf., Figure 5 (right).

What is especially of interest here is how well these responses couple with the Fourier series expansion of the pressure $S_{PP}(\boldsymbol{\alpha}_{m'n'})$. It is maximum at convective wavenumbers close to $\alpha_{m'} = \omega/U_c$ and also at wavenumbers $\alpha_{n'} = 0$, decreasing steadily with increasing $\alpha_{n'}$, see Figure 6. Modes $\Psi_{m,n=1}$ are more likely to couple well as they respond strongly to wave excitation with $\boldsymbol{\alpha}_{m',n'=0,1}$.

The aerodynamic coincidence, occurring when the bending and the convective wave speeds are equal, is at 546·4 Hz. Modes with resonant frequencies close to this frequency will respond greatly, as can be seen later in the response of, for example, mode $\Psi_{m=9,n=1}$

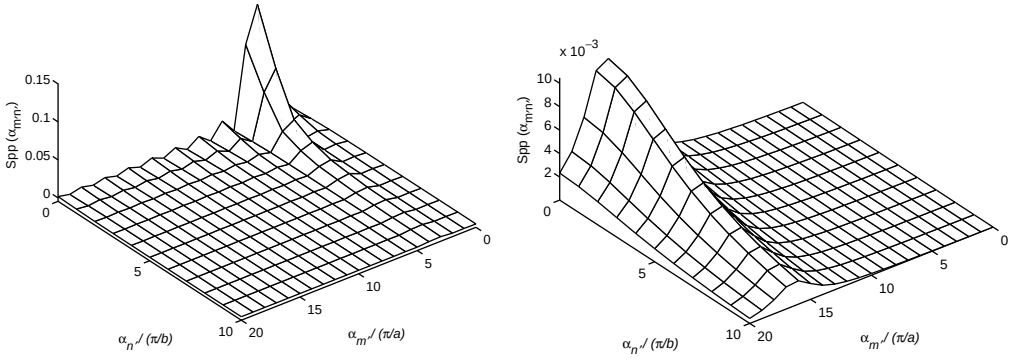

Figure 6. Fourier series coefficients, equations (39) and (40), describing Corcos model for TBL wall pressure cross-correlation. Left, 201 Hz. Right, 981 Hz.

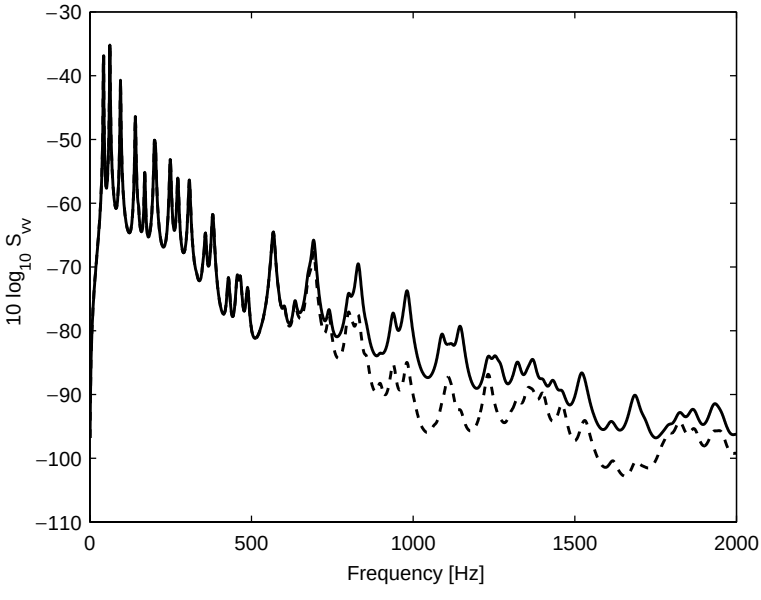

Figure 7. Velocity response to TBL excitation of a simply supported plate. (—) Modal analysis with 30 longitudinal and 15 transverse modes and equally spectral FEM with $M' = 20$ and $N' = 10$; (– –) spectral FEM with $M' = 10$ and $N' = 10$.

with natural frequency $f_{mn} = 567$ Hz in Figure 7. The modes $\Psi_{m=8,n=2}$ and $\Psi_{m=6,n=3}$ do not respond as much, because they do not couple well to a distributed pressure with exponential dependence $\alpha_{m',n'=0}$ or $\alpha_{m',n'=1}$. For low frequencies the energy of the TBL excitation is mainly at these low wavenumbers, cf., Figure 6. With higher frequencies the spatial correlation of the TBL excitation in the y direction decreases rapidly and the Fourier series expansion spectra become flatter. The wavenumber description starts to resemble "rain on the roof" in the y direction and hence all transverse modes in the y direction will start to couple equally well to $S_{PP}(\alpha_{m'n'})$. In the x direction a similar

phenomenon can be observed, but the spatial correlation decreases less rapidly with frequency in the direction of the flow, cf., Corcos formulation with $c_x < c_y$.

In Figures 5 and 6 values are only shown for positive $\alpha_{m'}$ and $\alpha_{n'}$. Negative values of $\alpha_{n'}$ are not shown due to symmetry with respect to $\alpha_{n'=0}$, whereas negative values of $\alpha_{m'}$ were excluded as $S_{PP}(\boldsymbol{\alpha}_{m'n'})$ has its maximum around the convective peak, i.e., $\alpha_{m'} \approx \omega/U_c$, and is quite small for negative values of $\alpha_{m'}$. In the next section, though, all $\boldsymbol{\alpha}_{m',n'}$ were considered.

If the structure is small (and the frequency low), the response of separate modes can be analyzed in the wavenumber domain and directly compared with the TBL excitation. For large structures this approach is not very fruitful, as hundreds of modes will be present even at low frequencies. Of more interest then is to directly compare the spatial characteristics of the excitation to that of the response in the wavenumber domain.

5.3. COMPARISON WITH MODAL ANALYSIS

Figure 7 shows the calculated velocity response to TBL excitation using spectral FE and the data given in section 5.1. This result was compared with results from a modal analysis, outlined in section 4.4 and also initially (not shown here) with an approximate modal procedure, see reference [20]. Davies [20] assumption that $c_{x(y)} U_c/\omega \ll l_{x,(y)}$ was here only valid above approximately 300 Hz. Otherwise, the methods agreed well, with small relative differences.

From Figure 7 it is observed that, if the highest wavenumber $\boldsymbol{\alpha}_{M',N'}$, describing the TBL excitation, is less than the structural wavenumber of the higher order modes $\Psi_{M,N}$ that have cut on, the resulting velocity response is underestimated. Hence $M'$and N' should be

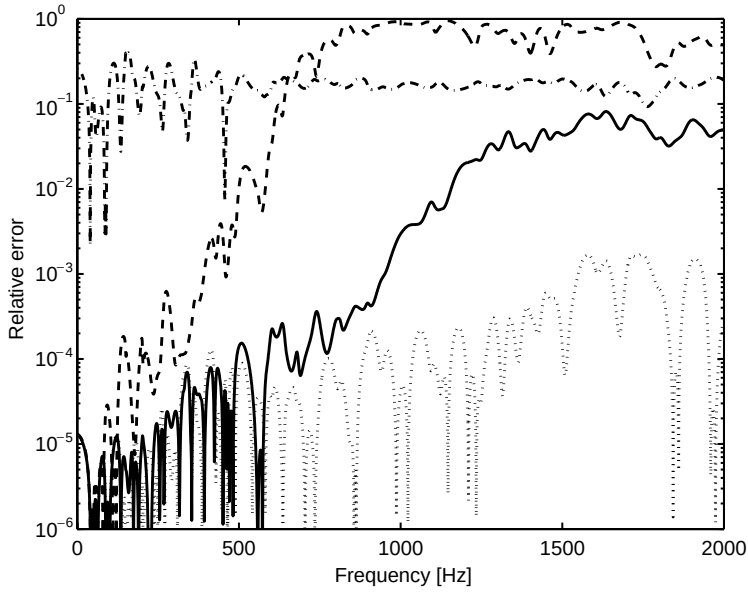

Figure 8. Relative error of the velocity response S_{vv}, where modal analysis is taken as datum solution. (– –) spectral FEM with $M' = 10$ and $N' = 10$; (—) spectral FEM with $M' = 20$ and $N' = 10$; (· · · · · ·) spectral FEM with $M' = 50$ and $N' = 30$; (–·–) modal analysis, where cross-modes were neglected.

chosen considering the structural wavenumbers of all higher order cut-on modes present at 2000 Hz. Here, this was satisfied by $M' = 20$ and $N' = 10$.

Figure 8 compares the relative error between the results calculated with the spectral FEM. As a datum solution, with four significant digits, the response given by the modal analysis was taken. To decrease the relative error below 0·1%, not only do the structural wavenumbers at 2000 Hz have to be considered, but also the wavenumber description of the TBL excitation, which at 2000 Hz requires approximately $M' = 50$ and $N' = 30$, due to the flatness of its spectra in the wavenumber domain. With this choice of parameters, the spectral FEM produced a result that had more significant digits than the datum solution and further comparison was meaningless. Also shown is the relative error of approximately 10–20% introduced if cross-modes are neglected in the modal analysis.

The spectral FEM was efficient compared to the modal analysis approach and only the neglect of cross-modes in the latter made the methods comparable in computational efficiency.

6. CONCLUSIONS

Previously, much attention had been directed to investigate the response of structures to TBL excitation. A new approach to this problem has been presented here which investigates the response in the wavenumber domain. First, the response of a plate to a distributed excitation with a complex exponential spatial dependence, i.e., a plane pressure wave, is calculated with the spectral FEM. The use of a particular integral allows for an exact calculation of this response, without recourse to modal analysis. Then the cross-spectral density of the TBL wall pressure cross-correlation is expressed as a finite exponential Fourier series. The structural response to each term in this series can be calculated with the spectral FEM and the total response is given by superposition. Hence using this approach the vibrational response of the plate to TBL excitation is determined.

The method presented is efficient compared to a modal analysis approach. The neglect of cross-modes would make the methods comparable in efficiency, but introduce an error of the order of 10–20% for the predicted auto-spectral density of the velocity in the frequency range investigated.

With the approach described, a direct comparison is possible between the spatial characteristics of the TBL excitation and of the structural response. This comparison reveals which modes will be excited more than others and how changes to the structure, or the TBL excitation, will influence the response of the structure. Many different descriptions of the TBL wall pressure are discussed in the literature, see reference [15], and these can be included in the formulation as long as they have a Fourier series expansion in the wavenumber domain.

The spectral FEM allows the equations of motion of a structure to be assembled and solved by using standard techniques of the finite element method. At present, the possibility of clamped boundary conditions along all edges is being investigated, where the governing wave equations are formulated with the methods outlined in reference [23].

The presented method should also apply to other complex structures. Finnveden *et al.* [24], for example, calculate the pipe response to a fully developed internal turbulent flow. The results are in excellent agreement with measurement results taken from reference [14].

REFERENCES

1. J. F. Wilby and F. L. Gloyna 1972 *Journal of Sound and Vibration* **23**, 443–466. Vibration measurements of an airplane fuselage structure. I. Turbulent boundary layer excitation.
2. P. M. Morse and H. Feshbach 1953 *Methods of Theoretical Physics*. New York: McGraw-Hill.
3. G. M. L. Gladwell 1966 *Journal of Sound and Vibration* **4**, 172–186. A variational formulation for damped acousto-structural problems.
4. S. Finnveden 1997 *Journal of Sound and Vibration* **199**, 125–154. Spectral finite element analysis of the vibration of straight fluid-filled pipes with flanges.
5. S. Finnveden 1994 *Acta Acustica* **2**, 461–482. Exact spectral finite element analysis of stationary vibrations in a rail way car structure.
6. S. Finnveden and R. J. Pinnington 2000 *Journal of Sound and Vibration* **229**, 147–182. A velocity method for estimating dynamic strain and stress in pipes.
7. R. S. Langley 1989 *Journal of Sound and* Vibration **135**, 319–331. Application of the dynamic stiffness method to the free and forced vibration of aircraft panels.
8. A. Y. T. Leung 2001 *Journal of Sound and Vibration* **242**, 377–395. Dynamic stiffness for structures with distributed deterministic or random loads.
9. R. Lundén and B. Åkesson 1983 *International Journal of Numerical Methods in Encineering* **19**, 431–449. Damped second order Rayleigh–Timoshenko beam vibration in space—an exact complex dynamic member stiffness matrix.
10. R. Lundén and B. Åkesson 1993 *International Journal of Numerical Methods in Encineering* **36**, 4267–4268. Letter to the editor, Some comments on: Damped second order Rayleigh–Timoshenko beam vibration in space—an exact complex dynamic member stiffness matrix.
11. J. F. Doyle 1997 *Wave Propagation in Structures*. New York: Springer-Verlag.
12. F. Birgersson 2000 *M.Sc. Thesis, ISVR, The University of Southampton*. Modelling with the dynamic stiffness and the spectral finite element methods for distributed sources.
13. M. Corcos 1967 *Journal of Sound and Vibration* **6**, 59–70. The resolution of turbulent pressure at the wall of a boundary layer.
14. C. Durant, G. Robert, P. J. T. Filippi and P. O. Mattei 2000 *Journal of Sound and Vibration* **229**, 1115–1155. Vibroacoustic response of a thin cylindrical shell excited by a turbulent internal flow: comparison between numerical prediction and experimentation.
15. W. K. Blake 1986 *Mechanics of Flow-induced Sound and Vibration*, Vols. 1 and 2. New York: Academic Press.
16. W. R. Graham 1997 *Journal of Sound and Vibration* **206**, 541–565. A comparison of models for the wavenumber frequency spectrum of turbulent boundary layer pressures.
17. D. E. Newland 1984 *An Introduction to Random Vibration and Spectral Analysis*. New York: Longman.
18. M. Petyt 1990 *Introduction to Finite Element Vibration Analysis*, Cambridge: Cambridge University Press.
19. G. Strang 1996 *Introduction to Applied Mathematics*, Wellesley: Wellesley-Cambridge Press; Chapter 5.
20. H. G. Davies 1971 *Journal of the Acoustical Society of America* **49**, 878–889. Sound from TBL-excited panels.
21. W. R. Graham 1996 *Journal of Sound and Vibration* **192**, 101–120. Boundary layer induced vibration in aircraft. Part 1: the flat plate model.
22. T. Dahlberg 1999 *Journal of Sound and Vibration* **228**, 157–176. The effect of modal coupling in random vibration analysis.
23. U. Orrenius and S. Finnveden 1996 *Journal of Sound and Vibration* **198**, 203–224. Calculation of wave propagation in rib-stiffened plate structures.
24. S. Finnveden, F. Birgersson and N. S. Ferguson 2001 *Proceedings of InterNoise* 2001, Vol. 5, 2497–2502. Modelling with the spectral FEM for turbulence excitation of cylindrical pipes.

APPENDIX A: EVALUATION OF THE LAGRANGIAN

Equation (25) is evaluated by substituting the functions X_n and X_n^a (defined by equations (23) and (24)) and their respective derivatives into it. The different terms are

similar and can be evaluated separately and then added together. Here a general term in equation (25) is evaluated to show the procedure:

$$
\begin{aligned}
&\int_{-l_x}^{l_x} (\mathrm{d}^r X_n^a/\mathrm{d}x^r)^{\mathrm{T}} B_i (\mathrm{d}^s X_n/\mathrm{d}x^s)\,\mathrm{d}x \\
&\quad = B_i \int_{-l_x}^{l_x} \{((\mathbf{K}.^\wedge r).*\mathrm{e}^{\mathbf{K}x-\mathbf{K}_p l_x}\mathbf{A}\mathbf{W}_n^a + c_n(\boldsymbol{\alpha}_{\mathbf{K}}.^\wedge r).*\mathrm{e}^{\boldsymbol{\alpha}_{\mathbf{K}}x-\boldsymbol{\alpha}_{\mathbf{K}_p} l_x}\mathbf{W}_{np})^{\mathrm{T}} \\
&\qquad \times ((\mathbf{K}.^\wedge s).*\mathrm{e}^{\mathbf{K}x-\mathbf{K}_p l_x}\mathbf{A}\mathbf{W}_n + c_n(\boldsymbol{\alpha}_{\mathbf{K}}.^\wedge s).*\mathrm{e}^{\boldsymbol{\alpha}_{\mathbf{K}}x-\boldsymbol{\alpha}_{\mathbf{K}_p} l_x}\mathbf{W}_{np})\}\,\mathrm{d}x \\
&\quad = B_i \int_{-l_x}^{l_x} \{((\mathbf{K}.^\wedge r).*\mathrm{e}^{\mathbf{K}x-\mathbf{K}_p l_x}\mathbf{A}\mathbf{W}_n^a)^{\mathrm{T}}((\mathbf{K}.^\wedge s).*\mathrm{e}^{\mathbf{K}x-\mathbf{K}_p l_x}\mathbf{A}\mathbf{W}_n) \\
&\qquad + ((\mathbf{K}.^\wedge r).*\mathrm{e}^{\mathbf{K}x-\mathbf{K}_p l_x}\mathbf{A}\mathbf{W}_n^a)^{\mathrm{T}}(c_n(\boldsymbol{\alpha}_{\mathbf{K}}.^\wedge s).*\mathrm{e}^{\boldsymbol{\alpha}_{\mathbf{K}}x-\boldsymbol{\alpha}_{\mathbf{K}_p} l_x}\mathbf{W}_{np})\}\,\mathrm{d}x + R \\
&\quad = \mathbf{W}_n^{a\mathrm{T}}\mathbf{A}^{\mathrm{T}} B_i((\mathbf{K}.^\wedge r)^{\mathrm{T}}(\mathbf{K}.^\wedge s)).*\left(\int_{-l_x}^{l_x} (\mathrm{e}^{\mathbf{K}x-\mathbf{K}_p l_x})^{\mathrm{T}}\mathrm{e}^{\mathbf{K}x-\mathbf{K}_p l_x}\,\mathrm{d}x\right)\mathbf{A}\mathbf{W}_n \\
&\qquad + \mathbf{W}_n^{a\mathrm{T}}\mathbf{A}^{\mathrm{T}} B_i((\mathbf{K}.^\wedge r)^{\mathrm{T}}(\boldsymbol{\alpha}_{\mathbf{K}}.^\wedge s)).*\left(\int_{-l_x}^{l_x} (\mathrm{e}^{\mathbf{K}x-\mathbf{K}_p l_x})^{\mathrm{T}}\mathrm{e}^{\boldsymbol{\alpha}_{\mathbf{K}}x-\boldsymbol{\alpha}_{\mathbf{K}_p} l_x}\,\mathrm{d}x\right)\mathbf{W}_{np}c_n + R, \qquad \text{(A1)}
\end{aligned}
$$

where $(.*)$ and $(.^\wedge)$ denote element-wise multiplication and power respectively (as in MATLAB). $(\mathbf{v}_1\mathbf{v}_2)^{\mathrm{T}} = \mathbf{v}_2^{\mathrm{T}}\mathbf{v}_1^{\mathrm{T}}$ was used and also that dot products are commutative. R contains terms that do not depend on $\mathbf{W}_n^a$. The first variation of the Lagrangian with respect to the test functions X_n^a is to be zero. Because the terms in R do not contribute to this variation, they are eliminated. All the terms given in equation (25) are evaluated in this way and added to get the final expression. The first variation of this new Lagrangian with respect to $\mathbf{W}_n^{a\mathrm{T}}$ is to be zero, producing the following system of linear equations in the nodal displacement $\mathbf{W}_n$ the first of which is just equation (26):

$$\mathbb{D}_n\mathbf{W}_n = \mathbf{F}_n, \qquad \text{(A2)}$$

$$\mathbb{D}_n = \mathbf{A}^{\mathrm{T}}\frac{b}{2}(\mathbf{Q_1}.*\mathbf{E_I}(\mathbf{K},\mathbf{K}_p,\mathbf{K},\mathbf{K}_p))\mathbf{A}, \qquad \text{(A3)}$$

$$\mathbf{F}_n = -\mathbf{A}^{\mathrm{T}}\frac{b}{2}(\mathbf{Q_2}.*\mathbf{E_I}(\mathbf{K},\mathbf{K}_p,\boldsymbol{\alpha}_{\mathbf{K}},\boldsymbol{\alpha}_{\mathbf{K}p}))\mathbf{W}_{np}c_n + \mathbf{A}^{\mathrm{T}}\frac{b}{2}\mathbf{E_I}(\mathbf{K},\mathbf{K}_p,-\mathrm{i}\alpha_x,0)p_0P_n(\alpha_y), \qquad \text{(A4)}$$

where

$$
\begin{aligned}
\mathbf{Q_1} &= B_1(\mathbf{K}.^\wedge 2)^{\mathrm{T}}(\mathbf{K}.^\wedge 2) + B_2(\mathbf{K}.^\wedge 2)^{\mathrm{T}}(\mathbf{K}.^\wedge 0) \\
&\quad + B_2(\mathbf{K}.^\wedge 0)^{\mathrm{T}}(\mathbf{K}.^\wedge 2) + B_3(\mathbf{K}.^\wedge 1)^{\mathrm{T}}(\mathbf{K}.^\wedge 1) + B_4(\mathbf{K}.^\wedge 0)^{\mathrm{T}}(\mathbf{K}.^\wedge 0), \\
\mathbf{Q_2} &= B_1(\mathbf{K}.^\wedge 2)^{\mathrm{T}}(\boldsymbol{\alpha}_{\mathbf{K}}.^\wedge 2) + B_2(\mathbf{K}.^\wedge 2)^{\mathrm{T}}(\boldsymbol{\alpha}_{\mathbf{K}}.^\wedge 0) \\
&\quad + B_2(\mathbf{K}.^\wedge 0)^{\mathrm{T}}(\boldsymbol{\alpha}_{\mathbf{K}}.^\wedge 2) + B_3(\mathbf{K}.^\wedge 1)^{\mathrm{T}}(\boldsymbol{\alpha}_{\mathbf{K}}.^\wedge 1) + B_4(\mathbf{K}.^\wedge 0)^{\mathrm{T}}(\boldsymbol{\alpha}_{\mathbf{K}}.^\wedge 0). \qquad \text{(A5)}
\end{aligned}
$$

The matrix generating function $\mathbf{E_I}$ is defined as

$$\mathbf{E_I}(\mathbf{K},\mathbf{K}_p,\boldsymbol{\alpha}_{\mathbf{K}},\boldsymbol{\alpha}_{\mathbf{K}p}) = \int_{-l_x}^{l_x} (\mathrm{e}^{\mathbf{K}x-\mathbf{K}_p l_x})^{\mathrm{T}}(\mathrm{e}^{\boldsymbol{\alpha}_{\mathbf{K}}x-\boldsymbol{\alpha}_{\mathbf{K}_p} l_x})\,\mathrm{d}x \qquad \text{(A6)}$$

so that its entries are given by

$$(\mathbf{E_I})_{ij} = ((e^{(\mathbf{K})_i(+l_x)-(\mathbf{K}_p)_i l_x})(e^{(\boldsymbol{\alpha}_\mathbf{K})_j(+l_x)-(\boldsymbol{\alpha}_{\mathbf{K}p})_j l_x}) - (e^{(\mathbf{K})_i(-l_x)-(\mathbf{K}_p)_i l_x})(e^{(\boldsymbol{\alpha}_\mathbf{K})_j(-l_x)-(\boldsymbol{\alpha}_{\mathbf{K}p})_j l_x}))/((\mathbf{K})_i + (\boldsymbol{\alpha}_\mathbf{K})_j). \quad \text{(A7)}$$

APPENDIX B: DYNAMIC STIFFNESS METHOD FOR A SIMPLY SUPPORTED PLATE

For a plate excited by a harmonic point force $F_0 e^{i\omega t}$ at $\mathbf{s}_1 = (x_s, y_s)$, instead of a distributed force as in equation (3), the governing wave equation is given by

$$D\left(\frac{d^4 X_n}{dx^4} - 2k_n^2 \frac{d^2 X_n}{dx^2} + k_n^4 X_n\right) - \varrho h \omega^2 X_n = \frac{2F_0}{b} \sin(k_n y_s)\delta(x - x_s). \quad \text{(B1)}$$

Except at x_s, the solution is given by the complementary solution, detailed in equation (6),

$$X_n = \begin{cases} X_{n-} = \sum_{i=1}^4 A_{ni} e^{k_{ni} x}, & x < x_s, \\ X_{n+} = \sum_{i=1}^4 B_{ni} e^{k_{ni}(x-a)}, & x > x_s, \end{cases} \quad \text{(B2)}$$

where a is the length of the plate. The boundary conditions for a simply supported plate at $x = 0$ and a are

$$X_n = d^2 X_n / dx^2 = 0. \quad \text{(B3)}$$

At location x_s, the displacement and its first and second derivatives are continuous, i.e.,

$$X_{n-} = X_{n+}, \quad dX_{n-}/dx = dX_{n+}/dx, \quad d^2 X_{n-}/dx^2 = d^2 X_{n+}/dx^2 \quad \text{for } x = x_s. \quad \text{(B4)}$$

Another continuity condition is obtained by integrating equation (B1) with respect to x from $x_s - \varepsilon$ to $x_s + \varepsilon$ for infinitesimal ε:

$$[d^3 X_{n+}/dx^3 - d^3 X_{n-}/dx^3]_{x=x_s} = \frac{2F_0 \sin(k_n y_s)}{Db}. \quad \text{(B5)}$$

Given these conditions it is possible to solve the eight unknown parameters A_{ni} and B_{ni} in equation (B2) and thus describe the motion of the plate. An alternative approach is to use the result by Langley [7, equation (13)] to describe the motion of one plate element and then couple two plate elements.